

Bragg Diffraction from Crystallized Ion Plasmas

W. M. Itano,^{*} J. J. Bollinger, J. N. Tan,[†] B. Jelenković,[‡]

X.-P. Huang, D. J. Wineland

(Version 6.0, 30 January 1998)

Single crystals of a one-component plasma were observed by optical Bragg diffraction. The plasmas contained 10^5 to 10^6 single-positive beryllium-9 ions ($^9\text{Be}^+$) at particle densities of 10^8 to 10^9 per cubic centimeter. In approximately spherical plasmas, single body-centered cubic (bcc) crystals or, in some cases, two or more bcc crystals having fixed orientations with respect to each other were observed. In some oblate plasmas, a mixture of bcc and face-centered cubic ordering was seen. Knowledge of the properties of one-component plasma crystals is required for models of white dwarfs and neutron stars, which are believed to contain matter in that form.

Plasmas, the ionized states of matter, are usually hot and gaseous. However, a sufficiently cold or dense plasma can be liquid or solid. A one-component plasma (OCP) consists of a single charged species embedded in a uniform, neutralizing background charge (1). Aside from its intrinsic interest as a simple model of matter, the OCP may be a good model for some dense astrophysical plasmas (2), such as the crusts of neutron stars or the interiors of white dwarfs, where the nuclei are embedded in a degenerate electron gas. According to calculations, a classical, infinite OCP freezes into a bcc lattice when the Coulomb coupling parameter

$$\Gamma \equiv \frac{1}{4\pi\epsilon_0} \frac{e^2}{a_{\text{WS}}k_{\text{B}}T}, \quad (1)$$

is approximately equal to 170 (3). Here, ϵ_0 is the permittivity of the vacuum, e is the charge of an ion, k_{B} is Boltzmann's constant, T is the temperature, and a_{WS} is the Wigner-Seitz radius, defined by $4\pi a_{\text{WS}}^3/3 = 1/n_0$, where n_0 is the particle density; Γ is the ratio of the Coulomb potential energy of neighboring ions to the kinetic energy per ion.

Ion plasmas can be confined and brought to thermal equilibrium in Penning traps. Such systems have static thermal equilibrium properties equivalent to those of an OCP, where the magnetic field

takes the place of the background charge (4–6). Calculations (7) and experiments (8) for approximately spherical plasmas having $N \approx 10^3$ to 10^4 ions show concentric shell structures, dominated by surface effects. Calculations by Dubin and O'Neil (9,10) suggest that a bcc lattice might begin to form in the center when the number of concentric shells is greater than about 30, which corresponds, for a spherical plasma, to $N \approx 10^5$. Ordered structures of tens of thousands of ions have been observed in a radio-frequency (rf) quadrupole storage ring (11) and in a linear rf trap (12) but, because of the elongated shapes of these structures, surface effects dominated and bulk structure was not observed.

Tan *et al.* have reported Bragg diffraction patterns from laser-cooled ions in a Penning trap (13). For approximately spherical plasmas with 200,000 ions or more, the patterns were consistent with bcc ordering but not with face-centered cubic (fcc) ordering. However, the Bragg patterns were smeared into circles by the rotation of the plasma about the magnetic field axis, so it was not possible to distinguish between scattering by a single crystal and scattering by several crystals or to determine the orientation of the crystals. Here we report the observation of time-resolved (stroboscopic) Bragg diffraction patterns, from which the effect of the plasma rotation is removed (14).

In our experiment (Fig. 1), the $^9\text{Be}^+$ ions were confined in a cylindrical Penning trap, consisting of an electrostatic quadrupolar potential and a uniform magnetic field $B = 4.465$ T, parallel to the z axis. The radial electric field leads to a rotation, at frequency ω_r , of the plasma about the z axis. For a given N , an equilibrium state of the plasma can be parameterized by T and ω_r (4–6). In the limit of low T , approached in our experiments, the plasmas are uniform-density spheroids. For $N = 10^6$, a spherical plasma at a typical density of $4 \times 10^8 \text{ cm}^{-3}$ has a diameter of 1.7 mm.

The ions are cooled by a laser beam propagating along the z axis and tuned slightly lower in frequency than a hyperfine-Zeeman component of the $2s^2S_{1/2}$ to $2p^2P_{3/2}$ resonance at 313 nm. The laser power is approximately 50 μW and is focused at the ion plasma to a diameter of about 0.5 mm. We estimate that $T \lesssim 10$ mK (15,16). For a typical value of $n_0 = 4 \times 10^8 \text{ cm}^{-3}$, this results in $\Gamma \gtrsim 200$. A series of lenses forms an image of the diffraction pattern

Time and Frequency Division, National Institute of Standards and Technology, Boulder, CO 80303, USA.

^{*}To whom correspondence should be addressed. E-mail: witano@nist.gov

[†]Present address: Frequency & Time Systems, Beverly, MA 01915, USA.

[‡]On leave from the Institute of Physics, University of Belgrade, Yugoslavia.

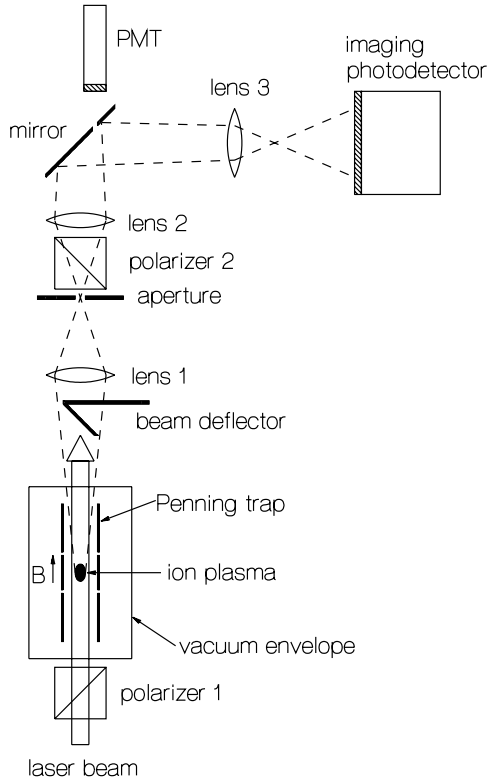


FIG. 1.: Experimental setup. Laser light is directed through the ion plasma in the Penning trap. A diffraction pattern is created at a plane beyond lens 2, where rays that are parallel leaving the plasma are focused to a point. A mirror, placed near that plane, deflects the light to an imaging photodetector. An aperture placed inside a hole in the mirror allows diffracted light to be detected by a photomultiplier tube (PMT). The aperture is placed off the axis of the optical system, so the PMT generates a timing signal as the diffraction pattern rotates.

on an imaging photodetector.

We used two methods to derive a timing signal for stroboscopic detection of the Bragg diffraction patterns. The first (passive method) is based on detecting a photon from a diffracted beam after it has passed through an aperture (Fig. 1). The second (active method) is based on phase-locking the rotation of the plasma to an applied rotating electric field (17,18).

Two types of imaging detectors were used. One (the MCP-RA detector) is an imaging photomultiplier tube (PMT) based on a microchannel-plate (MCP) electron multiplier and a multielectrode resistive anode (RA) for position sensing. For each photon, the position coordinates are derived from the current pulses collected from the different parts of the RA. The other is a charge-coupled device (CCD) camera coupled to an electronically gateable image intensifier.

Time-integrated diffraction patterns were ob-

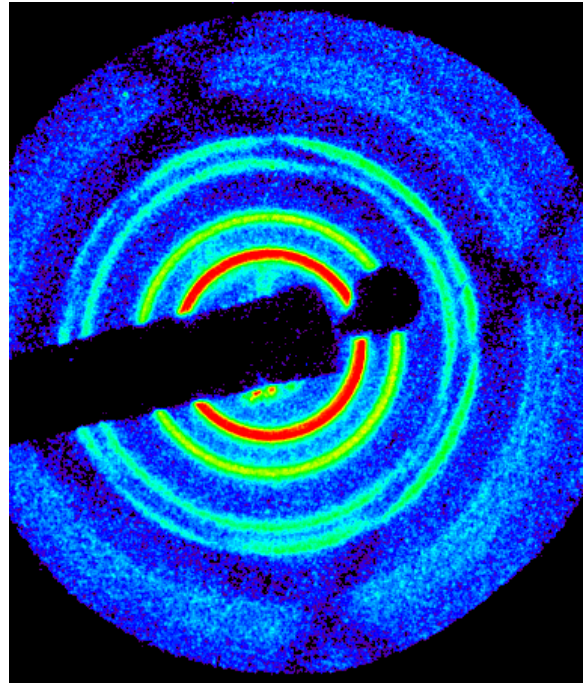


FIG. 2.: Time-integrated Bragg diffraction pattern obtained with the CCD camera. Rotation of the plasma causes the diffraction spots to be smeared into circles. The long rectangular shadow is due to the laser beam deflector. The small circular shadow is due to the hole in the mirror. The four linear shadows forming a large square are due to a wire mesh. Here, $\omega_r = 2\pi \times 128$ kHz, $n_0 = 3.90 \times 10^8$ cm $^{-3}$, $N = 5 \times 10^5$, $\alpha = 1.00$, and $2r_0 = 1.35$ mm.

tained with both the MCP-RA detector and the CCD camera. Before attempting to observe crystal diffraction patterns, we tuned the frequency of the laser beam from several gigahertz to ~ 10 MHz below resonance, causing T to vary from above to below the liquid-solid transition temperature. The duration of the frequency sweep was about 10 to 30 s. About 30% of the time, we observed a pattern consisting of several sharp rings, indicating that a crystal had been formed (13,14). Fig. 2, which is consistent with a bcc lattice rotating about a $\langle 100 \rangle$ (four-fold symmetry) axis (19), is an example of such a pattern.

In order to compare quantitatively the observed Bragg diffraction pattern to a calculated one, it is necessary to know n_0 , which can be determined from ω_r [equation 10 of Bollinger *et al.* (6)]. In (13), ω_r and n_0 were determined from the aspect ratio $\alpha = z_0/r_0$, where $2r_0$ and $2z_0$ are respectively the radial and axial diameters of the plasmas [equation 16 of Bollinger *et al.* (6)]. The uncertainty in ω_r determined by fitting the side-view images is $\sim 5\%$. If there are discrete Bragg diffraction peaks, ω_r can be determined accurately (to about 0.1%) from time correlations between scattered photons (Fig. 1). A typical correlation spectrum is shown in figure 4(a)

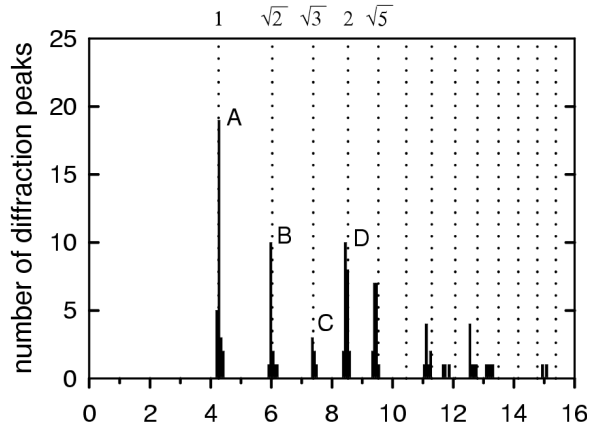


FIG. 3.: Histogram representing the numbers of peaks (not intensities) observed as a function of qa_{ws} , where $\mathbf{q} = \mathbf{k}_s - \mathbf{k}_i$ is the difference between the incident (\mathbf{k}_i) and scattered (\mathbf{k}_s) photon wave vectors. We analyzed 30 Bragg diffraction patterns from two approximately spherical plasmas having 270,000 and 470,000 ions. The dotted lines show the expected peak positions, normalized to the center of gravity of the peak at A ($\{110\}$ Bragg reflections).

of Tan *et al.* (14).

As reported in (13), 14 time-integrated Bragg diffraction patterns were analyzed for an approximately spherical plasma having 270,000 ions. Patterns for a larger data set, in which ω_r was determined by photon correlation, are shown in Fig. 3. The positions of the peaks agree with those calculated for a bcc lattice, to within the 2.5% uncertainty of the angular calibration. They disagree by about 10% with the values calculated for an fcc lattice. The ratios of the peak positions of the first five peaks agree to within about 1% with the calculated ratios for a bcc lattice. The scatter of the data is much reduced relative to that of figure 3 of Tan *et al.* (13), reflecting the more accurate ω_r determination.

In principle, Fig. 3 provides information on the orientations of the crystals. If the crystals formed with random orientations, we would expect Fig. 3 to show a greater number of diffraction peaks at C ($\{211\}$ Bragg reflections) than at D ($\{220\}$ Bragg reflections), whereas it actually shows the reverse. This data set showed a preference for alignment of the crystals with a $\langle 100 \rangle$ axis along the magnetic field direction. Preliminary observations indicate that the degree to which the magnetic field direction coincides with the symmetry axis of the trap electrodes influences the crystal orientations.

Tan *et al.* have noted (13) that not all of the diffraction rings allowed for various orientations of a bcc lattice were seen at any given time. This indicated that the portion of the plasma having bcc ordering included at most a few crystals rather than

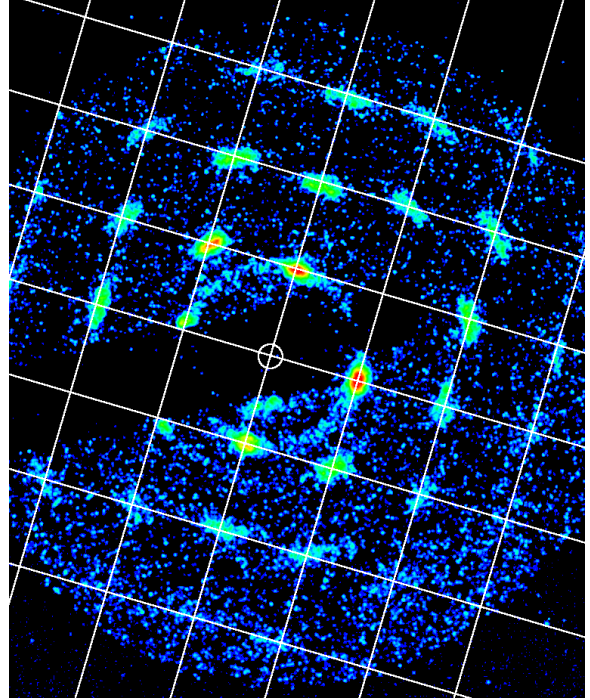


FIG. 4.: Time-resolved Bragg diffraction pattern of the same plasma as in Fig. 2. Here and in Figs. 5 and 6, the small open circle marks the position of the undeflected laser beam. A bcc lattice, aligned along a $\langle 100 \rangle$ axis, would generate a spot at each intersection of the grid lines overlaid on the image. The grid spacing corresponds to an angular deviation of 2.54×10^{-2} rad. Here, $\omega_r = 2\pi \times 125.6$ kHz, $n_0 = 3.83 \times 10^8$ cm $^{-3}$, $N = 5 \times 10^5$, $\alpha = 0.98$, and $2r_0 = 1.36$ mm.

many randomly oriented crystallites. Fig. 4 is an example of a time-resolved diffraction pattern obtained with the passive timing method and the CCD camera. In this case, the diffraction spots all line up on a square grid, consistent with a single bcc crystal oriented so that the incident laser beam is along a $\langle 100 \rangle$ axis. For these data, an angular calibration was made with an uncertainty of less than 1% with a mask. The agreement between the observed and calculated grid spacing was $\sim 1\%$.

In order for a diffracted beam to form, \mathbf{k}_s and \mathbf{k}_i must differ by a reciprocal lattice vector (Laue condition) (20). In a typical x-ray crystal diffraction case, satisfying the Laue condition for many spots requires that the incident radiation have a continuous range of wavelengths. Here, the Laue condition is relaxed because of the small size of the crystal, so a pattern is obtained even with monochromatic radiation. If the diameter of the region of the plasma having crystalline order is L , the mismatch in reciprocal space can be about $2\pi/L$. The diameter of this plasma was ~ 1.36 mm. In Tan *et al.* (13), approximate lower limits for L of 150 μ m and 240

μm were determined from the widths and intensities of the Bragg peaks, respectively. For this plasma, $a_{\text{WS}} = 8.5 \mu\text{m}$, and the cubic lattice spacing is $17 \mu\text{m}$. A cube $240 \mu\text{m}$ wide would be about 14 lattice spacings in diameter and would contain about 6000 ions.

We also observed patterns that were consistent with single bcc crystals nearly aligned along other directions, including $\langle 111 \rangle$, $\langle 115 \rangle$, $\langle 012 \rangle$, $\langle 113 \rangle$, $\langle 110 \rangle$, and $\langle 013 \rangle$. A pattern consistent with a single bcc crystal oriented along a $\langle 115 \rangle$ direction is shown in Fig. 5. Some time-resolved patterns were observed that were not consistent with a single crystal, but were consistent with two or more crystals having a fixed relative orientation.

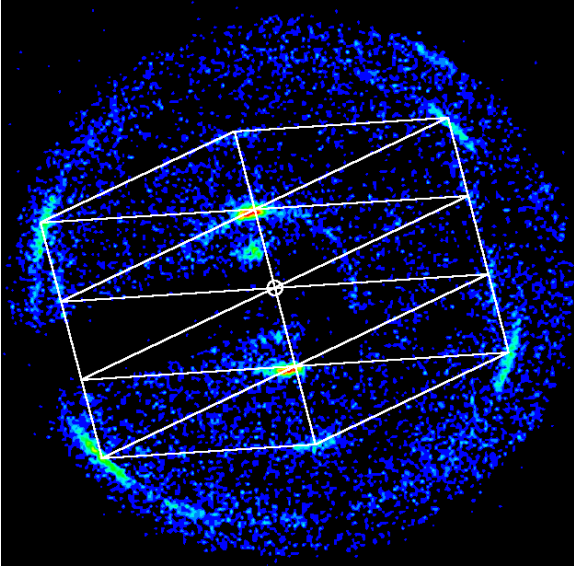


FIG. 5.: A Bragg diffraction pattern with two-fold symmetry. It matches the pattern expected for a bcc lattice oriented along a $\langle 115 \rangle$ direction. A diffraction spot is predicted at each intersection of the grid lines. The passive timing method and the MCP-RA detector were used. Here, $\omega_r = 2\pi \times 149 \text{ kHz}$, $n_0 = 4.53 \times 10^8 \text{ cm}^{-3}$, $N = 4 \times 10^5$, $\alpha = 1.20$, and $2r_0 = 1.12 \text{ mm}$.

With approximately spherical plasmas (α between 0.6 and 1.4), different diffraction patterns were observed on different cooling cycles. With more oblate plasmas, the same pattern was observed each time. A very oblate plasma resembles the planar geometry considered by Dubin and O'Neil (9,10), in which a stack of bcc (110) planes was predicted to have the lowest energy when there are about 60 or more planes. For some cases with fewer planes, a stack of fcc (111) planes has lower energy. In a time-resolved diffraction pattern from a plasma having $\alpha = 0.38$ (Fig. 6), the most intense diffraction spots form a rectangular array, consistent with a bcc lattice oriented along a $\langle 110 \rangle$ direction, that is, a stack of (110) planes. Weaker diffraction spots, forming a

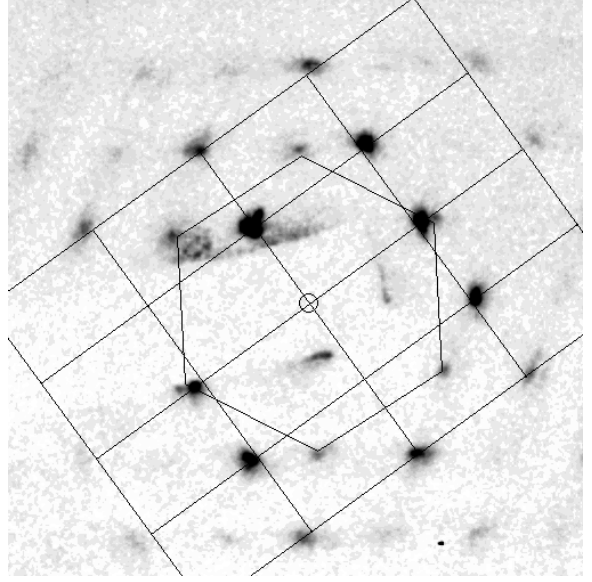


FIG. 6.: Time-resolved Bragg diffraction pattern showing a superposition of twofold and sixfold symmetric patterns. The rectangular grid connects the points for which diffraction spots are predicted for a bcc lattice oriented along a $\langle 110 \rangle$ direction. An fcc lattice oriented along a $\langle 111 \rangle$ direction would generate diffraction spots at the vertices of the hexagon. The orientation of the hexagon has been adjusted to fit the data, and it differs by about 3° from that of the rectangular grid. The active timing method and the CCD camera were used. Here, $\omega_r = 2\pi \times 70 \text{ kHz}$, $n_0 = 2.15 \times 10^8 \text{ cm}^{-3}$, $N = 5 \times 10^5$, and $2r_0 = 2.27 \text{ mm}$.

hexagon, are also seen. These appear at the lowest temperatures. The expected positions of the spots for the $\{220\}$ Bragg reflections of an fcc lattice oriented along a $\langle 111 \rangle$ direction, that is, a stack of (111) planes, are at the vertices of the hexagon overlay. An ideal hexagonal close-packed lattice, oriented along the $[001]$ direction, would generate the same hexagonal spot pattern. However, it would also generate another hexagonal spot pattern at a smaller radius, which is not observed.

Simulations of ion plasmas show hexagonal patterns resembling fcc (111) planes on the layers nearest the surface (7). The hexagonal diffraction pattern in Fig. 6 could be the result of scattering from surface layers, and the rectangular pattern could result from scattering from the central region. Some spots in Fig. 6 do not match either the rectangular grid or a hexagonal lattice. They may be due to scattering from a transition region that is neither bcc nor fcc. Further examination of oblate plasmas with different thicknesses may enable the transition from surface-dominated structure to bulk behavior in a finite, strongly coupled OCP to be studied.

REFERENCES AND NOTES

1. S. Ichimaru, *Rev. Mod. Phys.* **54**, 1017 (1982).
2. H. M. Van Horn, *Science* **252**, 384 (1991).
3. E. L. Pollock and J. P. Hansen, *Phys. Rev. A* **8**, 3110 (1973); W. L. Slattey, G. D. Doolen, H. E. DeWitt, *ibid.* **21**, 2087 (1980); *ibid.* **26**, 2255 (1982); S. Ogata and S. Ichimaru, *ibid.* **36**, 5451 (1987); G. S. Stringfellow and H. E. DeWitt, *ibid.* **41**, 1105 (1990); D. H. E. Dubin, *ibid.* **42**, 4972 (1990).
4. R. C. Davidson, *Physics of Nonneutral Plasmas* (Addison-Wesley, Redwood City, CA, 1990), chap. 3.3.
5. J. H. Malmberg and T. M. O'Neil, *Phys. Rev. Lett.* **39**, 1333 (1977).
6. J. J. Bollinger, D. J. Wineland, D. H. E. Dubin, *Phys. Plasmas* **1**, 1403 (1994).
7. A. Rahman and J. P. Schiffer, *Phys. Rev. Lett.* **57**, 1133 (1986); H. Totsuji, in *Strongly Coupled Plasma Physics*, F. J. Rogers and H. E. DeWitt, Eds. (Plenum, New York, 1987), p. 19; D. H. E. Dubin and T. M. O'Neil, *Phys. Rev. Lett.* **60**, 511 (1988); J. P. Schiffer, *ibid.* **61**, 1843 (1988); R. W. Hasse and V. V. Avilov, *Phys. Rev. A* **44**, 4506 (1991); J. P. Schiffer, in *Non-neutral Plasma Physics II*, F. Fajans and D. H. E. Dubin, Eds. (American Institute of Physics Conference Proceedings 331, AIP Press, New York, 1995), p. 191.
8. S. L. Gilbert, J. J. Bollinger, D. J. Wineland, *Phys. Rev. Lett.* **60**, 2022 (1988).
9. D. H. E. Dubin, *Phys. Rev. A* **40**, 1140 (1989).
10. D. H. E. Dubin and T. M. O'Neil, in *Strongly Coupled Plasma Physics*, S. Ichimaru, Ed. (Elsevier, Amsterdam, 1990), p. 189.
11. G. Birkl, S. Kassner, H. Walther, *Nature* **357**, 310 (1992).
12. M. Drewsen, C. Brodersen, L. Hornekær, J. S. Hangst, J. P. Schiffer, University of Aarhus, in preparation.
13. J. N. Tan, J. J. Bollinger, B. Jelenković, D. J. Wineland, *Phys. Rev. Lett.* **72**, 4198 (1995).
14. A preliminary report of the time-resolved detection has appeared [J. N. Tan, J. J. Bollinger, B. Jelenković, W. M. Itano, D. J. Wineland, in *Physics of Strongly Coupled Plasmas*, Proceedings of the International Conference, Binz, Germany, W. D. Kraeft and M. Schlages, Eds. (World Scientific, Singapore, 1996), p. 387].
15. J. J. Bollinger and D. J. Wineland, *Phys. Rev. Lett.* **53**, 348 (1984).
16. L. R. Brewer, J. D. Prestage, J. J. Bollinger, W. M. Itano, D. J. Larson, D. J. Wineland, *Phys. Rev. A* **38**, 859 (1988).
17. X.-P. Huang, F. Anderegg, E. M. Hollman, C. F. Driscoll, T. M. O'Neil, *Phys. Rev. Lett.* **78**, 875 (1997).
18. X.-P. Huang, J. J. Bollinger, T. B. Mitchell, W. M. Itano, *Phys. Rev. Lett.* **80**, 73 (1998).
19. The notation refers to the conventional cubic unit cells for the bcc and fcc lattices. A lattice plane specified by Miller indices h , k , and l is denoted by (hkl) ; a direction specified by components n_1 , n_2 , and n_3 is denoted by $[n_1n_2n_3]$; a set of planes that are equivalent by symmetry is denoted by $\{hkl\}$; and a set of directions that are equivalent by symmetry is denoted by $\langle n_1n_2n_3 \rangle$. See, for example, N. W. Ashcroft and N. D. Mermin, *Solid State Physics* (Saunders College, Philadelphia, 1976), chap. 5.
20. N. W. Ashcroft and N. D. Mermin, *ibid.*, chap. 6.
21. This manuscript is a work of the U.S. government. It is not subject to U.S. copyright. We acknowledge financial support from the Office of Naval Research.

29 August 1997; accepted 14 November 1997